Experimental tests of linear and nonlinear 3D equilibrium models in DIII-D

J.D. King[1,2], E.J. Strait[2], S.A. Lazerson[3], N.M. Ferraro[2], N.C. Logan[3], S.R. Haskey[4], J.-K. Park[3], J.M. Hanson[5], M.J. Lanctot[2], Y.Q. Liu[6], R. Nazikian[3], M. Okabayashi[3], C. Paz-Soldan[2], D. Shiraki[7], and A.D. Turnbull[2]

[1]*Oak Ridge Institute for Science Education, Oak Ridge, Tennessee 37830-8050, USA*

[2]*General Atomics, P.O. Box 85608, San Diego, California 92816-5608, USA*

[3]*Princeton Plasma Physics Laboratory, P.O. Box 451, Princeton, New Jersey 08543-0451, USA*

[4]*Plasma Research Laboratory, Research School of Physical Sciences and Engineering, The Australia National University, Canberra, ACT 0200, Australia*

[5]*Columbia University, 2960 Broadway, New York, New York 10027, USA*

[6] *Culham Centre for Fusion Energy, Culham Science Centre, Abingdon, Oxfordshire, OX14 3DB, United Kingdom*

[7]*Oak Ridge National Laboratory, P.O. Box 2008, Oak Ridge, Tennessee 37831, USA*

email of first author: kingjd@fusion.gat.com

Abstract. DIII-D experiments using new detailed magnetic diagnostics show that linear, ideal magnetohydrodynamics (MHD) theory quantitatively describes the magnetic structure (as measured externally) of three-dimensional equilibria resulting from applied fields with toroidal mode number $n = 1$, while a nonlinear solution to ideal MHD force balance, using the VMEC code, requires the inclusion of $n \geq 1$ to achieve similar

agreement. These tests are carried out near ITER baseline parameters, providing a validated basis on which to exploit 3D fields for plasma control development. Scans of the applied poloidal spectrum and edge safety factor confirm that low-pressure, n =1 non-axisymmetric tokamak equilibria are determined by a single, dominant, stable eigenmode. However, at higher beta, near the ideal kink mode stability limit in the absence of a conducting wall, the qualitative features of the 3D structure are observed to vary in a way that is not captured by ideal MHD.

PACS Nos.: 52.55.-s, 52.55.Fa, 52.30.Cv, 52.55.Tn, 52.65.Kj and 52.30.Ex

I. INTRODUCTION

Tokamaks are principally axisymmetric. However, global and local plasma stability is greatly affected by small toroidal asymmetries of the magnetic field. Understanding the physics of these small 3D distortions is needed to project control strategies to next step fusion reactors. The application of non-axisymmetric perturbations, intentionally or unintentionally, stimulates the plasma to respond by amplification and/or diamagnetic screening of the applied field [1]. The stable "plasma response" due to these effects represents a stable three-dimensional equilibrium, which is often assumed to depend only on the least stable eigenmode, with all other modes having negligible amplitude [2].

These 3D equilibria can have beneficial or deleterious effects on tokamak performance. For instance, error fields, resulting from imperfect machine construction, can reduce the stabilizing toroidal plasma rotation through viscous drag [3], resonant braking [4] and magnetic island formation [5]. Alternatively, 3D equilbria have been identified that allow neoclassical effects to accelerate plasma rotation and promote global stability [6]. Also, the pedestal pressure gradient and current density profiles in H-mode discharges [7] can be controlled using applied magnetic field asymmetries [8]. The physical mechanism giving rise to this control is only beginning to be understood [9], but it is observed that within a resonant window of pedestal safety factor [10], 3D fields may alter the edge transport, yielding pressure profiles that are stable to edge localized peeling-ballooning modes [11] (ELMs). This phenomenon is known as resonant magnetic perturbation (RMP) ELM suppression [12].

A number of numerical and physical models have been devised to computationally describe 3D equilibria in existing tokamaks. Unfortunately, appreciable disparities

between linear model formulations and a non-linear model (the VMEC code) [13] have persisted [14,15]. Determining if this discrepancy is due to non-linear physics or an issue with numerical implementation has, until now, remained an open question. Comparing the predicted external response with new magnetic measurements [16] spanning most of the poloidal extent of DIII-D allows the principal physics responsible for 3D equilibria to be identified, and ipso facto the validity of individual models to be tested.

The empirical correction of toroidal mode number $n = 1$ error fields in DIII-D is consistent with the hypothesis that a 3D equilibrium is principally determined by a single dominant kink mode that amplifies the external non-axisymmetric field [17]. In this single-mode description [18,19] the plasma 3D structure only depends on the structure of the dominant eigenmode, and not on the details of the external 3D field. This implies that any externally applied poloidal spectrum, with some toroidal coupling to the dominant mode, can eliminate the error induced kink response [20]. Despite widespread success of the single-mode description for error field correction and other applications, direct observation confirming the invariance of poloidal mode structure with the applied poloidal spectrum has been lacking. Here we present confirmation of this structural rigidity for low beta, rapidly rotating discharges with $n = 1$ fields. However, at pressures near the no-wall ideal stability limit (the beta limit in the absence of a stabilizing conducting boundary), the 3D equilibrium transitions to a qualitatively different structure suggesting a possible breakdown of the single-mode model.

This work provides a quantitative comparison of detailed magnetic plasma response measurements [16] with multiple model predictions to assess the validity of each physical

model and numerical implementation describing 3D equilibria. To assess the domain of validity of the model predictions, these tests span a diverse range of applied poloidal field spectra, and a variety of plasma pressures and current profiles. The method of experimentally generating and measuring 3D equilibria in the DIII-D tokamak is described in Sec. II. Also, the preparation of model inputs is explained. In Sec. III a brief introduction of each physical model is provided. Linear and non-linear computations of the response are compared with detailed structural measurements in section IV. Section V shows q_{95} and poloidal spectral dependencies are accurately described by linear ideal MHD and are consistent with a single stable eignenmode. This ideal MHD description is seen to break down as pressures are increased beyond the no-wall ideal stability limit in section VI. Finally, a brief discussion and summary is presented in Sec. VII.

II. EXPERIMENTAL METHOD

Observations of tolerably small deviations from toroidal symmetry in tokamaks ($\delta B/B<10^{-3}$) have been previously studied using a variety of diagnostic and experimental techniques [21-23]. Here we examine the stable plasma response to externally applied non-axisymmetric (n=1) fields using new detailed magnetic measurements of 3D tokamak equilibria [16]. The application of these fields relies on two active sets of 6 "picture-frame" coils inside the DIII-D tokamak [24], referred to as I-coils. These coils may be connected to power supplies in circuits allowing the application of toroidal mode numbers n = 1, 2 and 3. An illustration of the I-coils, and the 3D equilibrium they are expected to generate, is shown in Fig. 1. The color contours correspond to the amplitude of the field component normal to a toroidally axisymmetric flux surface (δB_n). Toroidal effects lead to a strong asymmetry between large and small major radius sides of the

torus, with eigenmodes generally having a shorter poloidal wavelength on the small-radius side – also referred to as the high-field side (HFS). We therefore focus on this HFS region of detailed eigenstructure. The locations of new magnetic sensors are illustrated in blue in Fig. 1(a). To improve measurement statistics the $n = 1$ applied fields are rotated at 10 Hz. This allows synchronous Fourier detection of the external response [25].

DIII-D has two sets of I-coils, allowing the applied poloidal spectrum to be adjusted by changing the pitch of the applied field. Here pitch refers to the toroidal angle between two poloidally displaced I-coils that are applying the same field amplitude. This is also known as I-coil phasing and examples of 60˚, 180˚, 240˚ and 300˚ phasings are shown in Fig. 1(b). Also shown is the "un-rolled" low field side (LFS) vessel wall along with an $n = 1$ kink structure for a plasma with $q_{95} \sim 4.3$ (where q_{95} is the safety factor at the surface enclosing 95% of the poloidal flux). This alignment of the I-coil phasings with respect to the LFS kink mode, and the corresponding changes in mode stability and structure, are described in Sec. V and VI.

Understanding the stability and structure of 3D equilibria requires exploration of multiple key plasma parameters. Previous work has found that resistive wall mode (RWM) stability is reduced as pressure rises [26]. However, the structural dependence of 3D equilibria has not been observed to change significantly. How, or if, the structure depends on pressure is not known. To test this, normalized beta is scanned over a wide range of values relative to the no-wall stability limit (beta is the ratio of plasma pressure to magnetic field pressure and normalized beta is $\beta_N = \beta(aB/I)$, where a is the plasma minor radius, B is the toroidal field and I is the plasma current). Weakly shaped plasmas with low internal inductance (l_i) are used, so that the no-wall stability limit occurs at an

easily accessible value of β_N. While the kink mode is a global mode, not localized at one rational surface, in diverted H-mode plasmas the pitch of the mode, as observed externally at the LFS, is similar to that of the magnetic field near the plasma edge at the LFS. The internal plasma current profile determines the location of additional internal rational surfaces. During all parameter scans the q-profile was maintained essentially constant. Internal diamagnetic screening of applied fields at rational surfaces, where plasma resistivity is small, is implicitly included in some of the models tested, but no effort to directly measure this effect is presented in this paper. Finally, the poloidal spectrum of the applied field is known to impact the resulting response amplitude [27]. Considering a single dominant kink mode, when the upper and lower I-coils are both applying a normal field that is in phase with the poloidal eigenstructure, the amplification increases by an amount proportional to the degree of alignment. By adjusting the toroidal phase difference of the upper and lower I-coils (phasing) for constant plasma conditions the single mode model may be rigorously tested.

The measured and modeled final 3D equilibrium state is tested here; we do not consider the dynamics of the transition to this state. The EFIT code [28] is used to generate 2D experimental equilibrium reconstructions constrained by external magnetic data and radial profile measurements of n_e, T_e, T_i, and B-field pitch. Without including internal profile constraints the uncertainty in these EFIT reconstructions would be too great to make meaningful model comparisons [29]. This is because these 2D equilibria serve as an input for the linear models and an initial condition for the nonlinear model. For these 2D equilibrium reconstructions, the edge bootstrap current density ($j_{edge,\,BS}$) is not directly measured on DIII-D, requiring estimation using the Sauter model [30], which

approximates the $j_{edge,\ BS}$ with edge temperature and density gradient measurements. Work has shown this to be a reliable estimate [31], but intrinsic profile uncertainties must be taken into account to quantitatively compare with models. The uncertainty in the reconstructed current profiles may be determined by accounting for differences in the pedestal gradient terms. Scaling $j_{edge,\ BS}$ by a constant multiplier C_{boot} while holding total plasma current constant, a new free boundary equilbrium may be computed. The χ^2 values associated with multiple scaled equilibria are parabolically distributed with respect to C_{boot}. The width of the parabolic fit corresponds to the standard deviation of the reconstructed current profile according to the relation $\chi^2\left[C_{\text{boot}}\left(\chi_0^2\right)\pm\sigma\right]=\chi^2\left[C_{\text{boot}}\left(\chi_0^2\right)\right]+1$, where χ_0^2 is the minimum χ^2. This relation between the uncertainty and χ^2 is shown for an experimental equilibrium in Fig. 2(a). The reconstructed current density profiles for the minimum χ^2(C_{boot} = 0.96) and the ±1σ(C_{boot} = 1.04 and 0.88) are shown in Fig. 2(b). These profiles represent an effective error bar in the reconstructed current density.

The three equilibria corresponding to the optimum χ^2 value, and the ±1σ values are each modeled. The bounds of these model predictions outline an envelope of possible response values, seen for the VMEC code in Fig. 2(c). It is important to note that these response variations are due to the uncertainty in the experimental input and not an error in any particular model. This strategy for accounting for errors in reconstructed equilibria was determined based on analysis of the largest sensitivity for the 3D model predictions and known deficiencies in the diagnostic constraints for DIII-D tokamak equilibria.

III. 3D EQUILIBRIUM MODELS

It is unknown to what extent experimental 3D equilibria are the result of laminar "flux-frozen" (ideal) displacements, resistive formation of magnetic islands, or nonlinearly distorted field lines. Previous work has found that linear ideal MHD successfully predicts the outer midplane response for plasma pressure (β_N) below the no-wall stability limit [1]. Does this linear description capture the full structure at all poloidal locations, or does the 3D structure require non-linear considerations? Does finite resistivity need to be included to describe the observed plasma response? As pressure is increased beyond the no-wall limit, does the structure of the equilibrium change, and if so, is this a consequence of non-ideal effects?

To assess these possibilities, we consider 4 unique models. These models are all formulated to handle poloidally shaped tokamak geometry. The code names associated with each model are IPEC, MARS-F, M3D-C1, and VMEC. The IPEC code approximates the 3D equilibrium as a linear perturbation to an ideal (perfectly conducting) plasma. Comparing the IPEC predicted response with measurement at multiple poloidal locations allows us to determine if linear ideal MHD correctly predicts the 3D equilibrium. Similarly MARS-F computations neglecting resistivity provide an additional linear ideal MHD response prediction employing a numerical strategy different from IPEC. The M3D-C1 code is used to identify the potential impact of resistive and two-fluid effects. Finally the potential non-linear response is assessed using the VMEC code, which is a stellarator equilibrium solver that has been modified to solve 3D force balance in tokamaks.

The 2D equilibrium code EFIT [28], which solves the Grad-Shafranov equation, provides a starting point for all non-axisymmetric modeling. The solution to the Grad-

Shafranov equation may include non-ideal effects [32,33]. Here fast ion pressures, and other non-ideal effects, are included through separate transport calculations to modify the 1D profile inputs ahead of the equilibrium reconstruction. Additional inputs to EFIT include axisymmetric coil currents, Motional Stark effect pitch angle measurements [34], external magnetic sensor measurements [35], Thomson scattering profiles of electron density and temperature, and charge exchange recombination profiles of ion temperature.

The code VMEC [13] indirectly solves $j \times B = -\nabla p$ in full 3D. Specifically, VMEC minimizes the ideal MHD energy functional while maintaining a key topological constraint that all flux surfaces are nested. It is unique from the other models as it nonlinearly computes the helically altered flux surfaces, instead of assuming a linear perturbation to an initial axisymmetric field. The full 3D geometry of the perturbing I-coils, as well as axisymmetric coils, is included in the model and the measured experimental coil currents are used to compute the resulting 3D equilibrium state. The code is run with and without currents in the non-axisymmetric I-coils. The DIAGNO code [36] provides a method to calculate the fields outside the last closed flux surface, which is necessary to determine the detected field strength at the locations of the magnetic sensors. The difference is taken between the 2D (no I-coil) and 3D (with I-coils energized) predicted sensor measurements to isolate the 3D plasma response component along the wall.

IPEC [19] solves the time-independent ideal perturbed equilibrium by finding the linear combination of ideal MHD eigenmodes, computed by the stability code DCON [37], that is consistent with the applied fields. Because this is a purely ideal calculation the resonant Fourier components of the perturbed normal fields at rational surfaces are

completely shielded. This shielding highlights a shortcoming of the ideal plasma assumption, which is that singular currents arise at rational surfaces. To avoid non-physical Pfirsch-Schlüter currents associated with the Glasser effect [38,39] a narrow radial region near the rational surface must be "jumped". Note that these currents are only non-physical in the ideal limit. This jump limits the resolution of ideal calculations to factors greater than 10^{-5} times the plasma radius. However, the validity of MHD in general requires that spatial scales be larger than both the ion and electron gyroradius. Here we consider plasmas with gyroradii that are factors of 10^{-2} and 10^{-3} times the plasma radius, such that higher order effects, associated with Pfirsch-Schlüter currents, do not alter the response. Detailed studies have shown that global amplification computations, like those presented here, are insensitive to these local currents [40].

The MARS-F code [41,42] solves the set of linear single fluid MHD equations including plasma resistivity and toroidal rotation terms (the full system of equations is presented in Ref [43]). However, MARS-F can also be run with resistivity and rotation set to zero, as has been done in this paper, allowing for ideal MHD response calculations using a different numerical approach from the IPEC code. Specifically, the MARS-F code solves a forced eigenvalue problem for an applied external vacuum field spectrum. This vacuum field is modeled as a source surface current in the poloidal plane at the location of the I-coils. To account for induced eddy currents in the vacuum vessel wall, the MARS-F code includes a conformal resistive wall that is modeled as a thin-shell.

Here, M3D-C1 is used to solve the time-independent perturbed equilibrium using a compressible, linear, resistive, two-fluid model [44]. In other words, the linearized set of MHD equations is solved subject to boundary conditions imposed by the applied non-

axisymmetric fields. This is different from typical M3D-C1 computations, which use an initial-value strategy. M3D-C1 uses high-order finite elements in (R,Z) coordinates. The input resistivity profiles are empirically determined from the measured T_e profiles using the classical Spitzer resistivity model, which is based on electron-ion collisions. For the cases considered here, the viscosity and perpendicular thermal conductivity are each ~ 10 m^2/s. In general, the thermal conductivity is strongly anisotropic with $\chi_{//}/\chi_{\perp} \sim 10^6$. Unlike the ideal MHD codes, the $E \times B$ equilibrium rotation profiles are also used in the computation. These calculations also include a resistive wall of finite thickness and variable resistivity [45]. Unique from the other codes, the computational domain contains the X-point and the cold scrape-off layer (SOL) plasma.

Beyond experimental uncertainty, described in Section II, there are practical model limitations and sensitivities. The M3D-C1 model includes the open field-line region in its computational domain, and therefore may be sensitive to equilibrium conditions there; however all other models considered here do not extend beyond the separatrix, and treat the open-field line region as a perfect vacuum. For these codes, the axisymmetric equilibrium must be truncated inside the separatrix. Here, this truncation encloses 99.7% of the normalized poloidal flux such that the foot of the edge pressure pedestal is included. Truncated equilibria are ideal MHD unstable when the safety factor at the truncation surface (qa) is sufficiently close to a rational value m/n, where m is poloidal mode number and n is toroidal mode number. To obtain a finite solution, the ideal MHD codes (VMEC, IPEC, and MARS-F) require that the equilibrium be truncated such that qa ≠ m/n. An additional consideration is that truncation causes a small non-zero pressure gradient at the boundary. This gradient is not physical and the equilibrium must be

recomputed to ensure $\nabla p = 0$. This new equilibrium is computed using the CORSICA code [46].

IV. MULTIPLE MODEL VALIDATION

Despite the numerous numerical and physical models that have been devised to computationally describe 3D equilibria in tokamaks and stellarators, a lack of experimental constraints has permitted disparities between models to remain unresolved. Now, dedicated magnetic measurements [16], covering most of the poloidal extent of DIII-D, are beginning to provide definitive answers concerning the validity of these models and the 3D physics they predict.

Comparing the models mentioned in Sec. III with new 3D magnetic measurements shows that linear models accurately predict the plasma response near ITER baseline beta. In Fig. 3, the predicted and measured poloidal component of the plasma response (δB_p) is compared for all available poloidal locations on DIII-D. The regions along the LFS correspond to the 5 facets of the DIII-D vacuum vessel and the corresponding sharp variations in the response profiles are a consequence of the angle discontinuities at each corner of the machine. On the HFS, the machine is a cylinder such that there are no response discontinuities. The amplitude of the response is normalized to the perturbing field strength. The phase has been referenced to the lower DIII-D I-coil located at 30˚ in the machine toroidal angle. Each response profile is plotted versus the distance from the machine midplane, which can be seen above in Fig. 1(d), along with the approximate locations of the measurement sensor pairs (blue).

The amplitude profiles along the HFS show that the linear predictions of IPEC, MARS-F, and M3D-C1 computations generally agree with measurement. While some

differences are seen, this agreement between three unique physical and numerical formalisms is remarkable and required a careful simultaneous benchmarking effort to ensure each model used the same starting inputs. Indeed, it is found that the linear models can be quite sensitive to the axisymmetric equilibrium, and high-resolution equilibria are required to obtain quantitative agreement. Additional modeling with M3D-C1, considering only a single fluid, showed no appreciable difference in the response. Therefore two-fluid effects are not critical to this plasma and do not explain the differences seen between it and the ideal model predictions. This is also reasonable to expect since these discharges were rapidly rotating such that resistive effects would be minimal. Of particular importance are the IPEC and MARS-F linear ideal MHD predictions that quantitatively agree with measurement along the entire height of the HFS wall. This agreement continues onto the LFS, with the exception of the midplane, where both predictions differ from measurement by ~15%. However, the measurement falls between the two predictions. The plasma parameters for this discharge are comparable to those in the ITER baseline scenario, with β_N ~1.6 and $q_{95} \sim 3.3$.

The nonlinear VMEC code is also in good agreement with measurement; however higher order toroidal modes must be included in the computation [47]. Despite their inclusion, these higher order modes contribute less than 10% to the plasma response amplitude. For calculations only including the applied n = 1, VMEC over predicts the response. Similar comparisons of JET plasma boundary displacements resulting from n = 2 RMPs, show VMEC predictions differ with measurement by a factor of three [48]. Unlike the other three codes, the VMEC code does not resolve currents near rational surfaces, which should impact external response. However, the low order of this n = 1

perturbation gives rise to only a few enclosed rational surfaces, suggesting additional factors may be contributing to this discrepancy. This motivated additional studies that find a numerical artifact [49] at the magnetic axis. Specifically an erroneous $m = 1$, $n = 1$ current filament is predicted. This artifact dominates the response when zero beta plasmas are considered [50]. Though core localized, the amplitude of this current is sufficiently large to contribute to the external response at the vacuum vessel wall. The physical and/or numerical reason for requiring these higher toroidal mode numbers is still under investigation. We suspect the higher n modes permit the surfaces to distort near the edge, where it is believed the linear response begins to break down.

The simultaneous benchmarking of the four models with one another was carried out, however some differences between linear model predictions are still apparent. Discrepancies between M3D-C1 predictions and data may be due to a difference in the input 2D equilibrium. M3D-C1 requires a non-zero temperature in the scrape-off layer (SOL). To best match the truncated inputs used in the other models, an arbitrary non-zero temperature is reduced until the predicted response profile asymptotes. The resulting profile is presented in Fig 3. Unfortunately, measurements of the SOL temperature can provide no additional constraint, as their uncertainties are greater than this M3D-C1 edge temperature sensitivity. While the MARS-F and IPEC codes agree with data they do differ from one another slightly, which may be due to differences in the numerical strategy employed. Nevertheless, based on this comparison, we conclude ideal MHD is sufficient to describe this low beta case no matter the numerical formalism.

V. SINGLE MODE MODEL CONFIRMATION AT LOW PRESSURE

A. Changes in response as q_{95} is varied

The structure of any kink mode depends on the q-profile, and the least stable kink depends in part on q_{95}. Until now experiments have mostly assumed the presence of a single dominant kink mode, and that all other eigenmodes are far from marginal stability and therefore only weakly excited. If only a single eigenmode is important, any toroidal array of active coils can control the 3D equilibrium, as long as there is some coupling. Modifications to the poloidal alignment of the applied field only change the strength of the coupling and not the structure of the mode.

Previous work [27] has shown that aligning the pitch of the perturbing field with the kink mode perturbation along the LFS results in stronger LFS response, and that a phasing of 240˚ is better aligned with the ideal predicted kink mode when $q_{95} \sim 3$ than when $q_{95} \sim 4$. As mentioned in Sec. II, DIII-D has two sets of I-coils that allow the pitch of the applied field to be varied. If the 3D structure is determined by a single least stable eigenmode, then aligning the applied LFS perturbation with the LFS kink structure should result in stronger HFS response. In Fig. 4, the HFS modeled and measured peak amplitude is largest when the perturbing field is aligned with the least stable kink mode along the LFS, supporting the idea that these 3D equilibria each are dominated by of a single stable eigenmode. For both cases a constant $n = 1$ field is applied with phasing of 240˚. A constant $\beta_N = 1.3$ is maintained while q_{95} is stepped from 3.2 to 4.1. The peak HFS response is seen to be 35 % larger when $q_{95} = 3.2$ as compared to the less aligned $q_{95} = 4.1$ case.

The MARS-F ideal MHD model predictions are in quantitative agreement with measurement at most poloidal locations for both cases. Furthermore, the slope of the

phase along the height of the wall is greater for the higher q_{95} case, which is consistent with a smaller LFS poloidal pitch.

B. Changes in response as phasing is varied

To confirm that pressure and external field coupling only impact stability and not 3D equilibrium structure at values of beta less than the no-wall limit, three discharges are considered where both pressure and coupling are modified to maintain a constant plasma response. This provides a direct experimental test of the utility of the single dominant kink mode model. While maintaining q_{95} constant at 4.1 the measured response profiles along the HFS are compared. In Fig. 5, the HFS plasma response amplitude and phase are largely the same for these 3 discharges with significantly different conditions. Specifically, these discharges have been tuned to maintain approximately the same peak amplitude by simultaneously increasing the kink coupling (phasing) while decreasing the drive pressure (β_N). The LFS kink structure for these discharges is comparable to that seen in Fig. 1(b). The maximum kink alignment for this q_{95} is associated with applied fields having approximately 300˚ phasing. For the largest kink misalignment (180˚) and highest pressure (β_N = 2.1) the structure is nearly the same as is seen for kink alignment (300˚) and the lowest pressure (β_N = 1.7). Besides similar phase profiles the amplitude profiles all show two local maxima at around Z ~ - 0.1 m and Z ~ + 0.4 m.

These measurements confirm that the single mode model holds at low values of pressure. In other words, the same plasma structure is maintained despite applying different 3D field structure. This implies almost any coil set can cancel an error field of the same n number. The shot-to-shot variations in the profiles are likely due to slight differences in the q-profiles for each case, which change the location of rational surfaces

where fields are screened. Also, the case with 180˚ phasing shows a noticeable difference in the phase along the height of the wall. This shift in the phase is consistent with previous LFS observations near the no-wall limit [1] and suggest some non-ideal effects are beginning to play a role. Here the no-wall limit is estimated at $\beta_N \sim 2.2$. Despite these moderate differences, the structure of the modes is nearly identical. This provides direct evidence that only a single eigenmode exists for pressures less than the no-wall limit.

VI. HIGH PRESSURE RESPONSE TRANSITION

In the presence of a resistive wall and sufficient toroidal plasma rotation, the no-wall beta limit ($\beta_N^{\text{no-wall}}$) may be exceeded [51]. However no evidence of 3D equilibrium structural variation has previously been seen. In fact, previous LFS MHD spectroscopic measurements suggest the single mode model applies even when $\beta_N > \beta_N^{\text{no-wall}}$ [25].

However, for constant applied fields, new HFS mode structures are found to emerge as β_N exceeds the no-wall stability limit. For the discharges considered, $\beta_N^{\text{no-wall}} \sim 2.2$. In Fig. 6, the HFS amplitude profiles for 7 discharges scanning β_N for two different values of q_{95} are presented. Only the amplitude profiles are presented as the phase profiles show little variation from those presented in Fig. 4. For $\beta_N < \beta_N^{\text{no-wall}}$ the response scales by a constant multiplier. As the pressure approaches and exceeds $\beta_N^{\text{no-wall}}$ the structures for both values of q_{95} undergo a qualitative transition to a new 3D equilibrium. Specifically, for q_{95} = 4.2, [Fig. 6(a)] the two local maxima located at Z = -0.1 m and Z = +0.4 m assume a new state with a single maximum value peaked at Z = +0.3 m. For the q_{95} = 3.3 case, Fig. 6(b) shows different $\beta_N < \beta_N^{\text{no-wall}}$ profiles consisting of a single peak at Z = + 0.3 m and a plateau in the response for -0.3 m < Z < -0.1 m that transitions to two local maxima at Z = -0.4 m and Z = + 0.1 m.

The transition in the response for the q_{95} = 3.3 case occurs before the no-wall limit is surpassed suggesting non-ideal effects may be impacting mode stability even in an ideal stable regime.

Changes in the ideal-MHD response structure are expected if the underlying 2D equilibrium changes with pressure. For example, Shafranov shift [52] can modify the q-profile altering the radial location of the perturbed flux surfaces relative to the magnetic sensors. To determine if the observed structural transition is due to non-ideal effects the ideal response is computed.

Ideal MHD does not capture this pressure-driven eigenmode transition for either value of q_{95}. The computed ideal MHD stable response profiles are shown in Fig. 6(c,d) for uniformly scaled pressure profiles. To model this experiment, the pressures of the experimental equilibria for the β_N = 2.5 discharges were scaled down below the no-wall limit while maintaining other profile parameters largely constant. The poloidal structure is qualitatively different than the measured high beta response [Fig. 6(a,b) – black]. Also, the predicted response shows no appreciable variation as a function of pressure, instead the response uniformly scales. While there is some qualitative resemblance of the ideal predictions with the low beta response profiles for each q_{95}, there is not the same quantitative agreement seen in the previous cases where the actual experimental equilibria are used. The peak amplitude of the higher beta cases are much larger than seen in experiment, which is consistent with previous work showing that outboard midplane predictions diverge from measurement when the ratio $\beta_N/\beta_N^{\text{no-wall}} > 80\%$ [1]. The modest differences are likely due to variations in the experimentally realized q-profiles between the low and high beta cases in the scan. Specifically these ideal predictions include

changes in the q-profile associated with the high beta case, indicating non-ideal effects are required to explain this beta driven structural transition.

Based on these comparisons non-ideal effects modify not only the amplitude of the response but also the structure, for beta above the no-wall limit. It has been hypothesized that kinetic wave-particle interactions may modify a single eigenvector, which could explain the observed transition. However, further work has shown that the response variation is due to contributions by one or more additional stable eigenmodes [53], and is thought to be due to kinetic effects altering the relative mode stability such that multiple stable modes may be amplified. This multiple stable mode finding [53] is supported by previous observations of the loss of mode rigidity during unstable RWM growth and suppression in the NSTX and HBT-EP devices [54,55].

VII. DISCUSSION AND CONCLUSIONS

Early experimental [56] and analytical theory [57,58] work identified tokamak coil asymmetries as contributing to mode locking, and motivated efforts to eliminate 3D distortions. Concurrently, 3D fields were found to positively influence edge particle and heat fluxes, as well as impurity exhaust [59]. These competing impacts on tokamak plasma performance called for a deeper physical understanding.

This work identifies linear MHD as providing a valid basis for integrated 3D control development for maximizing tokamak performance. 3D equilibria arising from applied $n = 1$ fields are observed to respond in a purely ideal manner at low plasma pressure. The predictions of the IPEC linear ideal MHD code and the single-fluid MARS-F code both quantitatively agree with new detailed 3D magnetic response measurements at nearly every poloidal location on DIII-D. Specifically their domain of validity is near ITER

baseline parameters (q_{95} = 3.3 and β_N = 1.6). Although these findings are isolated to global n = 1 kink modes in H-mode discharges, recent validation efforts covering edge radially localized n = 3 perturbations show similar agreement with the MARS-F code in L-mode discharges [60], suggesting truly predictive capabilities may be close at hand.

In these lower pressure plasmas the 3D equilibria are dominated by a single eigenmode, and changes in the coupling strength (coil phasing) increase mode amplification, but have no impact on the structure of the mode. Similarly, plasma pressure only serves as a drive term for the least stable mode. It is important to note that these findings only confirm the physical concept that the form of a 3D equilibrium is defined by a single eigenmnode. The results presented here do not definitively validate the energy principle contained in the Boozer model [61], which has been challenged [62, 63, 64]. Nevertheless, a quantitative comparison in future DIII-D experiments, focused on measured plasma response changes as a function of the mode rotation, could provide this proof [65]. Furthermore, it is seen that this rigid mode description is not appropriate at pressures near the no-wall limit. At these higher pressures a qualitative transition is seen in the structure of the plasma response that is inconsistent with ideal MHD predictions. This implies that the coil geometry for n = 1 error field correction as designed in ITER will be more than sufficient during initial Q = 10 baseline operations, but steady state goals, calling for higher beta ($3.0 < \beta_N < 4.0$), may require consideration of non-ideal contributions to the poloidal structure of the plasma response.

The simultaneous optimization of 3D fields to correct error fields, impart torque, suppress ELMs and stabilize RWMs may be facilitated through the use of validated 3D models. Note that the tests reported here were carried out in rapidly rotating plasmas. In

future large volume tokamak reactor plasmas the moment of inertia is expected to be large, while neutral beam injected torque is expected to be small. In the absence of alternative torque sources, it follows that the plasma rotation in these reactors will be much less than the discharges considered here. It is thought that plasma rotation can significantly influence mode stability at low beta through finite resistivity at rational surfaces, and at high beta through kinetic resonances. Further validation work is needed to confirm the importance of these non-ideal effects.

Acknowledgment

This material is based upon work supported in part by the U.S. Department of Energy, Office of Science, Office of Fusion Energy Sciences, using the DIII-D National Fusion Facility, a DOE Office of Science user facility, under Awards DE-FC02-04ER54698, DE-AC05-06OR23100, DE-AC02-09CH11466, DE-FG02-04ER54761, and DE-AC05-00OR22725. DIII-D data shown in this paper can be obtained in digital format by following the links at https://fusion.gat.com/global/D3D_DMP. The authors wish to thank R.J. Buttery for encouraging concurrent benchmarking of all codes tested. We also express gratitude to A.H. Reiman for fruitful validation discussions.

References

[1] M. J. Lanctot, H. Reimerdes, A. M. Garofalo, M. S. Chu, J. M. Hanson, Y. Q. Liu, G. A. Navratil, I. N. Bogatu, Y. In, G. L. Jackson, R. J. La Haye, M. Okayabashi, J.-K. Park, M. J. Schaffer, O. Schmitz, E. J. Strait, and A. D. Turnbull, Phys. Plasmas **18**, 056121 (2011).

[2] J.-K. Park, M. J. Schaffer, J. E. Menard and A. H. Boozer, Phys. Rev. Lett. **99**, 195003 (2007).

[3] W. Zhu, S. A. Sabbagh, R. E. Bell, J. M. Bialek, M. G. Bell, B. P. LeBlanc, S. M. Kaye, F. M. Levinton, J. E. Menard, K. C. Shaing, A. C. Sontag, and H. Yuh, Phys. Rev. Lett. **96**, 225002 (2006).

[4] H. Reimerdes, A. M. Garofalo, E. J. Strait, R. J. Buttery, M. S. Chu, Y. In, G. L. Jackson, R. J. La Haye, M. J. Lanctot, Y. Q. Liu, M. Okabayashi, J.-K. Park, M. J. Schaffer and W. M. Solomon, Nucl. Fusion **49**, 115001 (2009).

[5] R. Fitzpatrick and T. C. Hender, Phys. Plasmas **1**, 3337 (1994).

[6] A. M. Garofalo, K. H. Burrell, J. C. DeBoo, J. S. deGrassie, G. L. Jackson, M. Lanctot, H. Reimerdes, M. J. Schaffer, W. M. Solomon, and E. J. Strait, Phys. Rev. Lett. **101**, 195005 (2008).

[7] F. Wagner, G. Becker, K. Behringer, D. Campbell, A. Eberhagen, W. Engelhardt, G. Fussmann, O. Gehre, J. Gernhardt, G. v. Gierke, G. Haas, M. Huang, F. Karger, M. Keilhacker, O. Klüber, M. Kornherr, K. Lacknerr, G. Lisitano, G. G. Lister, H. M. Mayer, D. Meisel, E. R. Müller, H. Murmann, H. Niedermeyer, W. Poschenrieder, H. Rapp, H. Röhr, F. Schneider, G. Siller, E. Speth, A. Stäbler, K. H. Steuer, G. Venus, O. Vollmer, and Z. Yü, Phys. Rev. Lett. **49**, 1408 (1982).

[8] T. E. Evans, R. A. Moyer, K. H. Burrell, M. E. Fenstermacher, I. Joseph, A. W. Leonard, T. H. Osborne, G. D. Porter, M. J. Schaffer, P. B. Snyder, P. R. Thomas, J. G. Watkins and W. P. West, Nature Physics **2**, 419 (2006).

[9] R. Nazikian, C. Paz-Soldan, J. S. deGrassie, D. Eldon, T. E. Evans, N. M. Ferraro, B. A. Grierson, R. J. Groebner, S. R. Haskey, C. Hegna, J. D. King, N. C. Logan, G. R. McKee, R. A. Moyer, M. Okabayashi, D. M. Orlov, T. H. Osborne, J-K. Park, T. L. Rhodes, M. W. Shafer, P. B. Snyder, W. M. Solomon, E. J. Strait, M. R. Wade, Phys. Rev. Lett. (submitted) (2014).

[10] P.B. Snyder, K.H. Burrell, H.R. Wilson, M.S. Chu, M.E. Fenstermacher, A.W. Leonard, R.A. Moyer, T.H. Osborne, M. Umansky, W.P. West, and X.Q. Xu, Nucl. Fusion **47**, 961 (2007).

[11] P. B. Snyder, H. R. Wilson, J. R. Ferron, L. L. Lao, A. W. Leonard, T. H. Osborne, A. D. Turnbull, D. Mossessian, M. Murakami, and X. Q. Xu, Phys. Plasmas **9**, 2037 (2002).

[12] T. E. Evans, R. A. Moyer, P. R. Thomas, J. G. Watkins, T. H. Osborne, J. A. Boedo, E. J. Doyle, M. E. Fenstermacher, K. H. Finken, R. J. Groebner, M. Groth, J. H. Harris, R. J. La Haye, C. J. Lasnier, S. Masuzaki, N. Ohyabu, D. G. Pretty, T. L. Rhodes, H. Reimerdes, D. L. Rudakov, M. J. Schaffer, G. Wang, and L. Zeng, Phys. Rev. Lett. **92,** 235004 (2004).

[13] S. P. Hirshman and J. C. Whitson, Phys. Fluids **26**, 3553 (1983).

[14] A. D. Turnbull, Nucl. Fusion, **52**, 054016 (2012).

[15] A. D. Turnbull, N. M. Ferraro, V. A. Izzo, E. A. Lazerus, J. K. Park, W. A. Cooper, S. P. Hirshman, L. L. Lao, M. J. Lanctot, S. Lazerson, Y. Q. Liu, A. Reiman, and F. Turco, Phys. Plasmas **20**, 056114 (2013).

[16] J. D. King, E. J. Strait, R. L. Boivin, D. Taussig, M. G. Watkins, J. M. Hanson, N. C. Logan, C. Paz-Soldan, D. C. Pace, D. Shiraki, M. J. Lanctot, R. J. La Haye, L. L. Lao, D. J. Battaglia, A. C. Sontag, S. R. Haskey, and J. G. Bak, Rev. Sci. Instrum. **85**, 083503 (2014).

[17] C. Paz-Soldan, R. J. Buttery, A. M. Garofalo, J. M. Hanson, R. J. La Haye, M. J. Lanctot, J. K. Park, W. M. Solomon and E. J. Strait, Nucl. Fusion **54**, 073013 (2014).

[18] A. H. Boozer, Phys. Rev. Lett. **86**, 5059 (2001).

[19] J.-K. Park, A. H. Boozer, A. H. Glasser, Phys. Plasmas **14**, 052110 (2007).

[20] M. Okabayashi, J. Bialek, A. Bondeson, M. S. Chance, M. S. Chu, A. M. Garofalo, R. Hatcher, Y. In, G. L Jackson, R. J. Jayakumar, T. H. Jensen, O. Katsuro-Hopkins, R. J. La Haye, Y. Q. Liu, G. A. Navratil, H. Reimerdes, J. T. Scoville, E. J. Strait, M. Takechi, A. D. Turnbull, P. Gohil, J. S. Kim, M. A. Makowski, J. Manickam and J. Menard, Nucl. Fusion **45**, 1715 (2005).

[21] R. A. Moyer, M. A. Van Zeeland, D. M. Orlov, A. Wingen, T. E. Evans, N. M. Ferraro, J. M. Hanson, R. Nazikian, M. R. Wade, and L. Zeng, Nucl. Fusion **52**, 123019 (2012).

[22] M. W. Shafer, E. A. Unterberg, D. M. Orlov, T. E. Evans, J. H. Harris, D. L. Hillis, R. Maingi, R. A. Moyer, R. Nazikian and A. Wingen, Nucl. Fusion **52**, 12200 (2012).

[23] D. Shiraki, S. M. Angelini, P. J. Byrne, B. A. DeBono, P. E. Hughes, J. P. Levesque, M. E. Mauel, D. A. Maurer, G. A. Navratil, Q. Peng, N. Rath, D. J. Rhodes, and C. C. Stoafer, Phys. Plasmas **20**, 102503 (2013).

[24] J. L. Luxon, Nucl. Fusion, **42**, 614 (2002).

[25] H. Reimerdes, M. S. Chu, A. M. Garofalo, G. L. Jackson, R. J. La Haye, G. A. Navratil, M. Okabayashi, J. T. Scoville, and E. J. Strait, Phys. Rev. Lett. **93**, 135002 (2004).

[26] H. Reimerdes, J. Bialek, M. S. Chance, M. S. Chu, A. M. Garofalo, P. Gohil, Y. In, G. L. Jackson, R. J. Jayakumar, T. H. Jensen, J. S. Kim, R. J. La Haye, Y. Q. Liu, J. E. Menard, G. A. Navratil, M. Okabayashi, J. T. Scoville, E. J. Strait, D. D. Szymanski and H. Takahashi, Nucl. Fusion **45**, 368 (2005).

[27] M. J. Lanctot, H. Reimerdes, A. M. Garofalo, M. S. Chu, Y. Q. Liu, E. J. Strait, G. L. Jackson, R. J. La Haye, M. Okabayashi, T. H. Osborne, and M. J. Schaffer, Phys. Plasmas **17**, 030701 (2010).

[28] L. L. Lao, J. R. Ferron, R. J. Groebner, W. Howl, H. St. John, E. J. Strait, and T. S. Taylor, Nucl. Fusion **30,** 1035 (1990).

[29] F.S. Zaitsev, D.P. Kostomarov, E.P. Suchkov, V.V. Drozdov, E.R. Solano, A. Murari, S. Matejcik, N.C. Hawkes, and JET-EFDA Contributors, Nucl. Fusion **51**, 103044 (2011).

[30] O. Sauter, C. Angioni and Y. R. Lin-Liu, Phys. Plasmas **6**, 2834 (1999).

[31] M. R. Wade, M. Murakami, and P. A. Politzer, Phys. Rev. Lett. **92**, 235005 (2004).

[32] F.L. Hinton and R.D. Hazeltine, Rev. Mod. Phys. **48**, 239 (1976).

[33] L.E. Zakharov and V.D. Shafranov, *Equilibrium of Current-Carrying Plasmas in Toroidal Configurations*, M.A. Leontovich Reviews of Plasma Physics, Vol. 11, Consultants Bureau, New York (1986).

[34] D. Wróblewski, K. H. Burrell, L. L. Lao, P. Politzer and W. P. West, Rev. Sci. Instrum. **61**, 3552 (1990).

[35] E. J. Strait, Rev. Sci. Instrum. **77**, 023502 (2006).

[36] S. A. Lazerson, S. Sakakibara and Y. Suzuki, Plasma Phys. Control. Fusion **55**, 025014 (2013).

[37] A. H. Glasser and M. S. Chance, Bull. Am. Phys. Soc. **42**, 1848 (1997).

[38] A.H. Glasser, J.M. Greene, and J.L. Johnson, Phys. Fluids **18**, 875 (1975).

[39] A.H. Glasser, J.M. Greene, and J.L. Johnson, Phys. Fluids **19**, 567 (1976).

[40] J.-K. Park, "Ideal Perturbed Equilibria in Tokamaks," Princeton University (2009).

[41] Yueqiang Liu, A. Bondeson, C. M. Fransson, B. Lennartson, and C. Breitholtz, Phys. Plasmas **7**, 3681 (2000).

[42] Yueqiang Liu, M. S. Chu, I. T. Chapman, and T. C. Hender, Phys. Plasmas **15**, 112503 (2008).

[43] Yueqiang Liu, A. Kirk, and E. Nardon, Phys. Plasmas **17**, 122502 (2010).

[44] N. M. Ferraro, Phys. Plasmas **19**, 056105 (2012).

[45] N. M. Ferraro, L. L. Lao, S. C. Jardin, J. D. King, M. W. Shafer, F. Zhang, Bull. Am. Phys. Soc. **59**, 15 (2014).

[46] J. Crotinger, "Corsica: A comprehensive simulation of toroidal magnetic fusion devices," Lawrence Livermore National Laboratory Technical Report UCRL-ID-126284 (1997).

[47] S.A Lazerson, J. Loizu, S. Hudson, A. Cerfon, G. McFadden, J. King, S. Hirshman, *The nonlinear plasma response in the continuously nested flux surface limit*, Poster – Sherwood Fusion Theory Conference (2015).

[48] I. T. Chapman, M. Becoulet, T. Bird, J. Canik, M. Cianciosa, W. A. Cooper, T. Evans, N. Ferraro, C. Fuchs, M. Gryaznevich, Y. Gribov, C. Ham, J. Hanson, G. Huijsmans, A. Kirk, S. Lazerson, Y. Liang, I. Lupelli, R. A. Moyer, C. Nührenberg, F. Orain, D. Orlov, W. Suttrop, D. Yadykin, Nucl. Fusion **54**, 083006 (2014).

[49] S. P. Hirshman, private communication.

[50] S. A. Lazerson, private communication.

[51] E. J. Strait, T. S. Taylor, A. D. Turnbull, J. R. Ferron, L. L. Lao, B. Rice, O. Sauter, S. J. Thompson, and D. Wróblewski, Phys. Rev. Lett. **74**, 2483 (1995).

[52] V.D. Shafranov, At. Energy **13,** 521 (1962).

[53] J. D. King, E. J. Strait, N. M. Ferraro, J. M. Hanson, S. R. Haskey, M. J. Lanctot, Y. Q. Liu, N. Logan, C. Paz-Soldan, D. Shiraki, and A. D. Turnbull, "Evidence of Multiple Kink Mode Contributions to Three-dimensional Equilibria in High Beta Tokamaks," to be submitted to Phys. Rev. Lett. (2015).

[54] S. A. Sabbagh, R. E. Bell, J. E. Menard, D. A. Gates, A. C. Sontag, J. M. Bialek, B. P. LeBlanc, F. M. Levinton, K. Tritz, and H. Yuh, Phys. Rev. Lett. **97**, 045004 (2006).

[55] T. Sunn Pedersen, D. A. Maurer, J. Bialek, O. Katsuro-Hopkins, J. M. Hanson, M. E. Mauel, R. James, A. Klein, Y. Liu and G. A. Navratil, Nucl. Fusion **47**, 1293 (2007).

[56] J. T. Scoville, R. J. La Haye, A. G. Kellman, T. H. Osborne, R. D. Stambaugh, E. J. Strait and T. S. Taylor, Nucl. Fusion, **31**, 875 (1991).

[57] A. Reiman and D. Monticello, Phys. Fluids B **3**, 2079 (1991).

[58] A. Reiman, and D. Monticello, Phys. Fluids B **3**, 2617 (1991).

[59] S. C. McCool, A. J. Wooton, A. Y. Aydemir, R. D. Bengtson, J. A. Boedo, R. V. Bravenec, D. L. Brower, J. S. deGrassie, T. E. Evans, S. P. Fan, J. C. Forster, M. S. Foster, K. W. Gentle, Y. X. He, R. L. Hickock, G. L. Jackson, S. K. Kim, M. Kotschenreuther, N. C. Luhmann Jr., W. H. Miner Jr., N. Ohayabu, D. M. Patterson, W. A. Peebles, P. E. Phillips, T. L. Rhodes, B. Richards, C. P. Ritz, D. W. Ross, W. L. Rowan, P. M. Schoch, B. A. Smith, J. C. Wiley, X. H. Yu and S. B. Zheng, Nucl. Fusion **29**, 547 (1989).

[60] S. R. Haskey, M. J. Lanctot, Y. Q. Liu, C. Paz-Soldan, J. D. King, B. D. Blackwell and O. Schmitz, Plasma Phys. Control. Fusion **57**, 025015 (2015).

[61] A.H. Boozer, Phys. Plasmas **6**, 831 (1999).

[62] V.D. Pustovitov, Phys. Plasmas **12**, 112504 (2005).

[63] A.H. Boozer, Phys. Plasmas **13**, 024703 (2006).

[64] V.D. Pustovitov, Phys. Plasmas **13**, 024704 (2006).

[65] V.D. Pustovitov, Phys. Plasmas **14**, 022501 (2007).

List of Figure Captions

Fig. 1. (Color online) Illustrations of (a) a full 3D n=2 normal field displacement δB_n for a three-dimensional tokamak equilibria perturbation (contours), DIII-D I-coils (green), new HFS magnetic sensor locations (blue), and (b) The "un-rolled" LFS δB_n due to am n=1 kink mode with q_{95} = 4.3 and overlaid I-coil locations (white) and I-coil phasings 60˚ (black), 180˚ (dark gray), 240˚ (light gray) and 300˚ (white).

Fig. 2. (Color online) (a) The magnetics χ^2 values for C_{boot} bootstrap current multipliers between 80% and 115%, a parabolic fit, and the 96%, 104%, and 88% C_{boot} values corresponding to equilibrium reconstructions optimum and +/- 1 σ, respectively (b) the $j_{//}$ for these error bars (c) the window of VMEC code predictions for these 3 $j_{//}$ inputs (d) A cross section the DIII-D tokamak showing an axisymmetric 2D equilibrium (red) and the poloidal locations of a new comprehensive set of magnetic field sensors (blue). Discharge 153485.

Fig. 3. (Color online) The amplitude (top) and phase (bottom) of the poloidal field component of the n = 1 plasma response measured (circles with error bars) and calculated by the MARS-F (blue), M3D-C1 (purple), IPEC (green) and VMEC (red) codes along the (a) LFS at 5 vacuum vessel surfaces, including those containing the upper (IU) and lower (IL) I-coils and (b) HFS of DIII-D. Discharge 153485.

Fig. 4. (Color online) MARS-F prediction and 3D magnetic measurement of the HFS plasma response amplitude and phase of a least stable kink (a) aligned with the external coil perturbation and (b) misaligned.

Fig. 5. (Color online) The amplitude (top) and phase (bottom) of the poloidal plasma response measured along the HFS (a) for $\beta_N < \beta_N^{no\text{-}wall}$ kink-aligned low beta (black, 153491.1650), mild kink-misalignment at slightly higher beta (blue, 153485.1400), and kink-misalignment at higher beta (green, 153486.1500).

Fig. 6. (Color online) The response amplitude profiles along the HFS for plasmas with phasing = 240˚ (a) measured for discharges with q_{95} = 4.2 – not kink aligned and β_N = 1.5 (red), 1.8 (blue), and 2.5 (black), (b) measured for discharges with q_{95} = 3.3 – kink aligned and β_N = 1.3 (red), 1.5 (blue), 2.0 (green), and 2.5 (black). Spline fits to the data are also plotted. (c) ideal MHD (MARS-F) predictions for discharges with q_{95} = 4.2 – not kink aligned and β_N = 1.5 (red), 1.8 (blue), and 2.0 (black), (d) ideal MHD (MARS-F) predictions for discharges with q_{95} = 3.3 – kink aligned and β_N = 1.5 (red), 1.9 (blue), 2.0 (green), and 2.1 (black). Discharges 153480 and 153485.

List of Figures

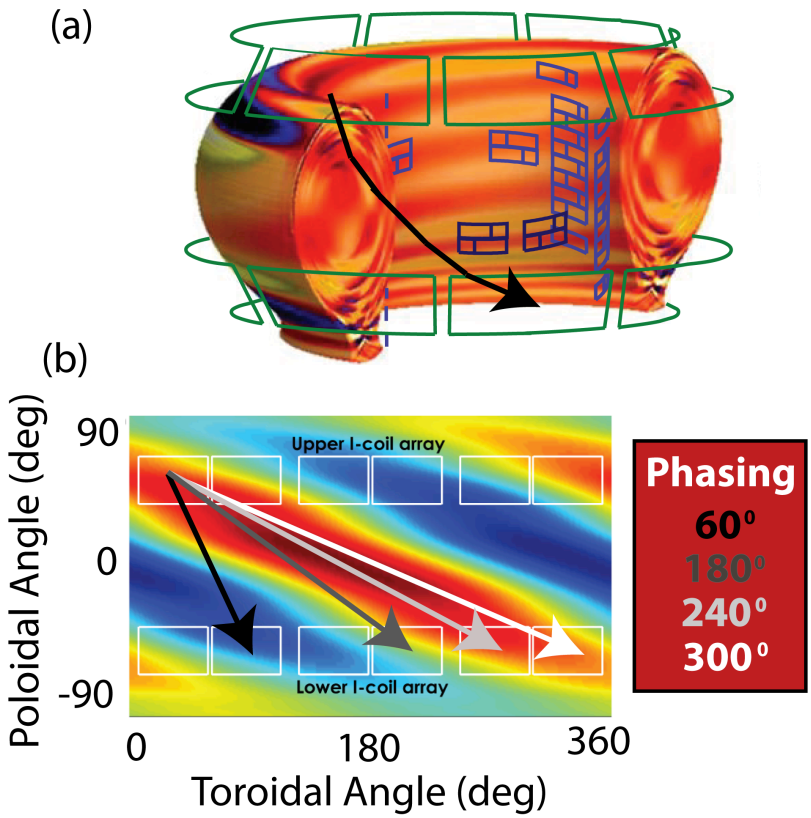

J.D. King Fig. 1

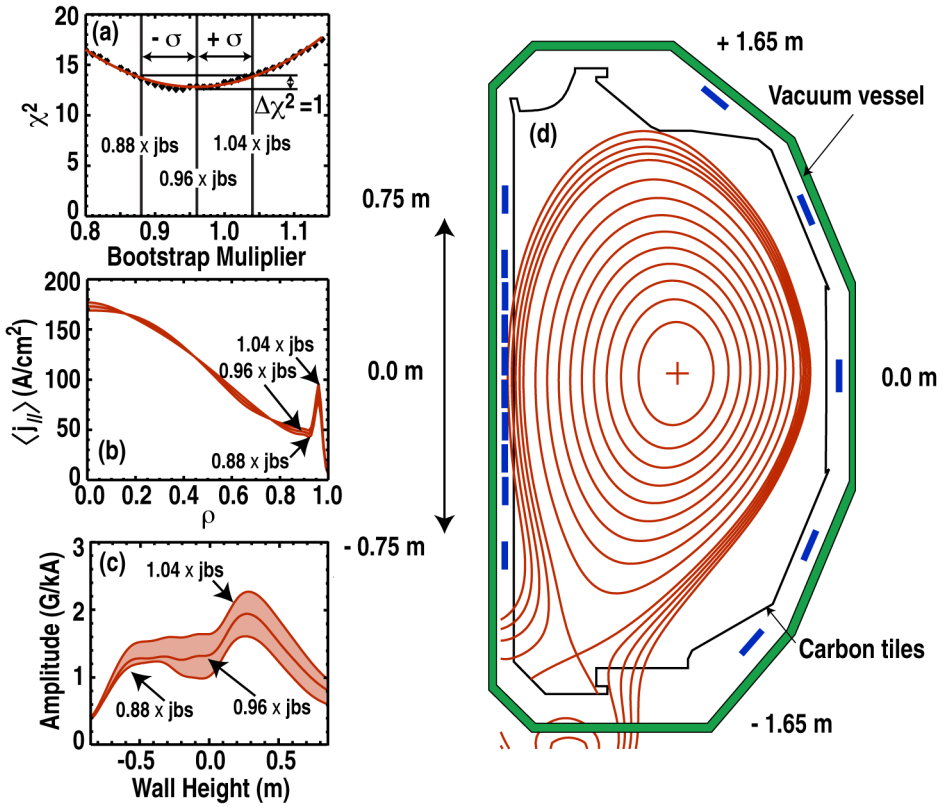
(a)
- σ
+ σ
$\Delta\chi^2 = 1$
0.88 x jbs
1.04 x jbs
0.96 x jbs
χ^2
Bootstrap Muliplier
(b)
1.04 x jbs
0.96 x jbs
0.88 x jbs
$\langle j_{//} \rangle$ (A/cm^2)
ρ
(c)
1.04 x jbs
0.88 x jbs
0.96 x jbs
Amplitude (G/kA)
Wall Height (m)
0.75 m
0.0 m
- 0.75 m
(d)
+ 1.65 m
Vacuum vessel
0.0 m
Carbon tiles
- 1.65 m

J.D. King Fig. 2

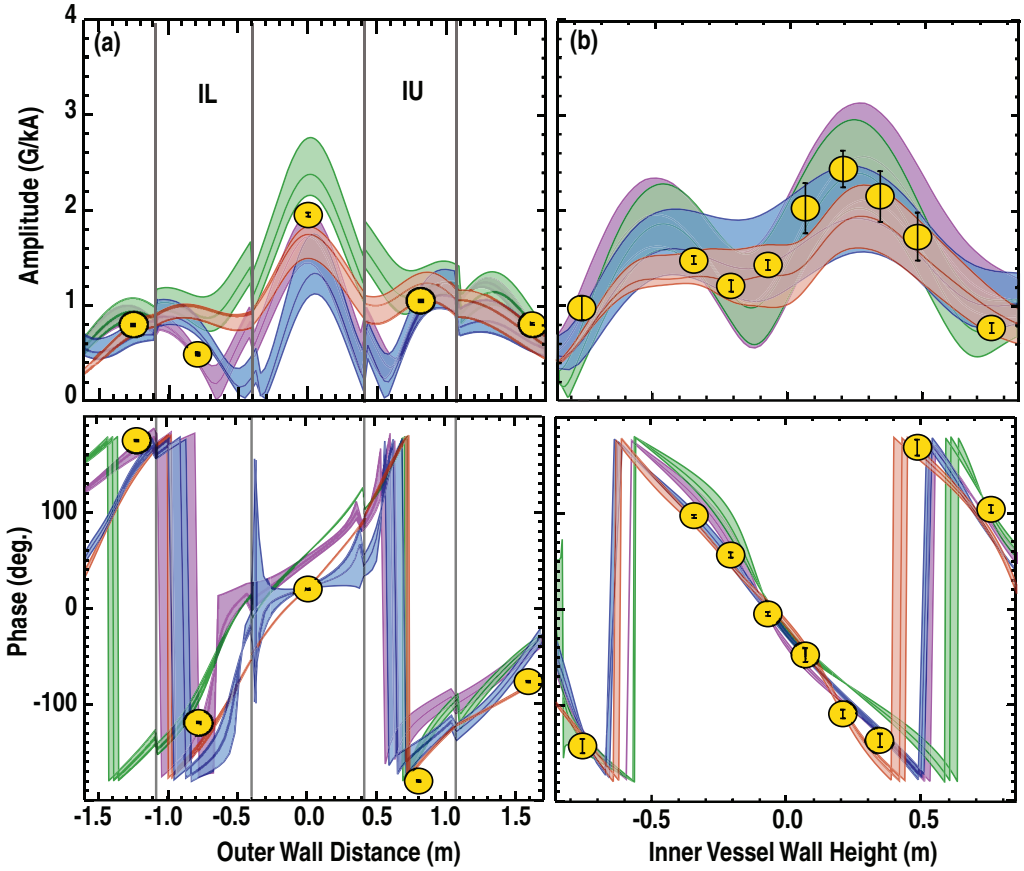
(a)
(b)
IL
IU
Amplitude (G/kA)
Phase (deg.)
Outer Wall Distance (m)
Inner Vessel Wall Height (m)

J.D. King Fig. 3

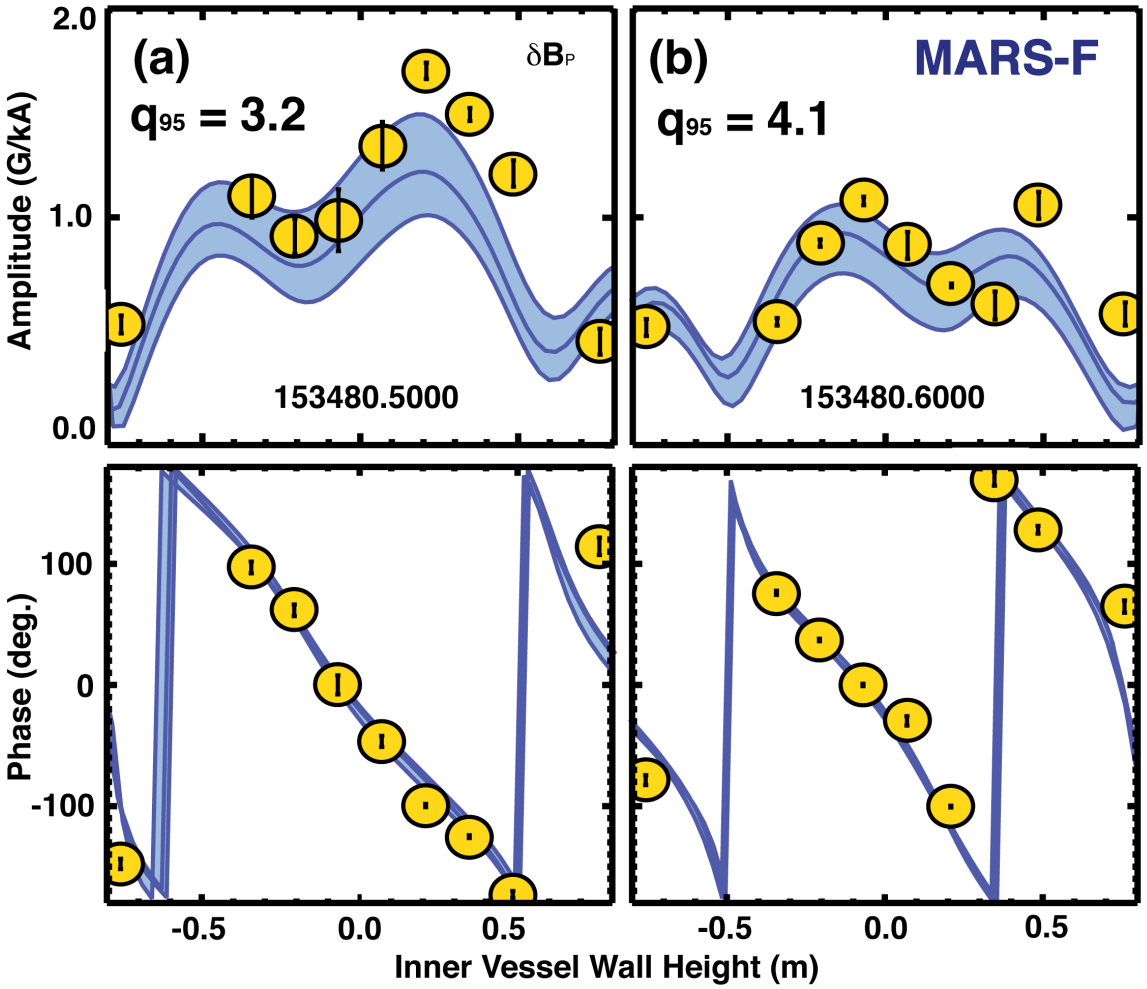
(a)
q_{95} = 3.2
δB_P
153480.5000
(b)
MARS-F
q_{95} = 4.1
153480.6000
Amplitude (G/kA)
2.0
1.0
0.0
Phase (deg.)
100
0
-100
-0.5
0.0
0.5
Inner Vessel Wall Height (m)

J.D. King Fig. 4

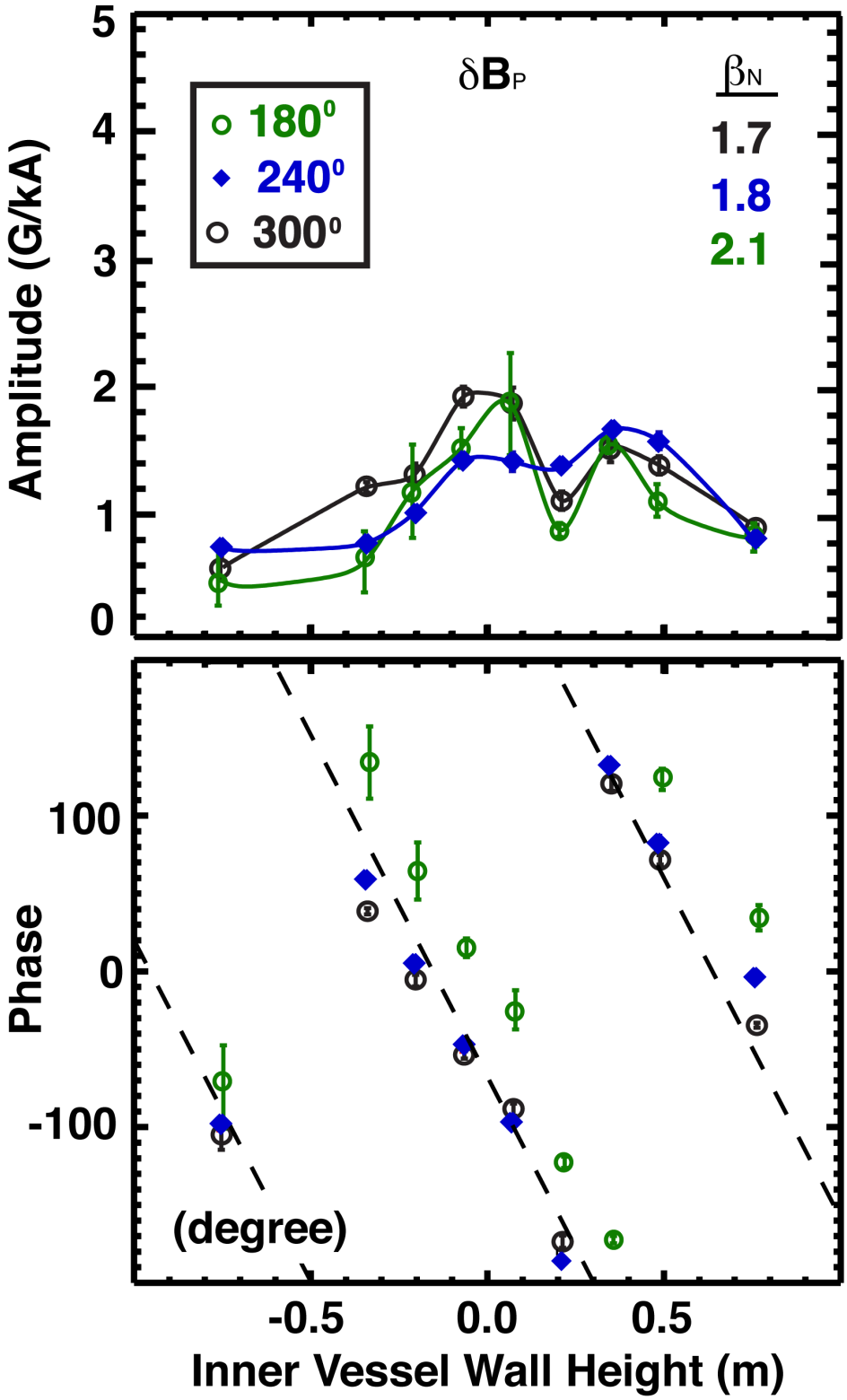
δBP
βN
1.7
1.8
2.1
180⁰
240⁰
300⁰
Amplitude (G/kA)
Phase
(degree)
Inner Vessel Wall Height (m)

J.D. King Fig. 5

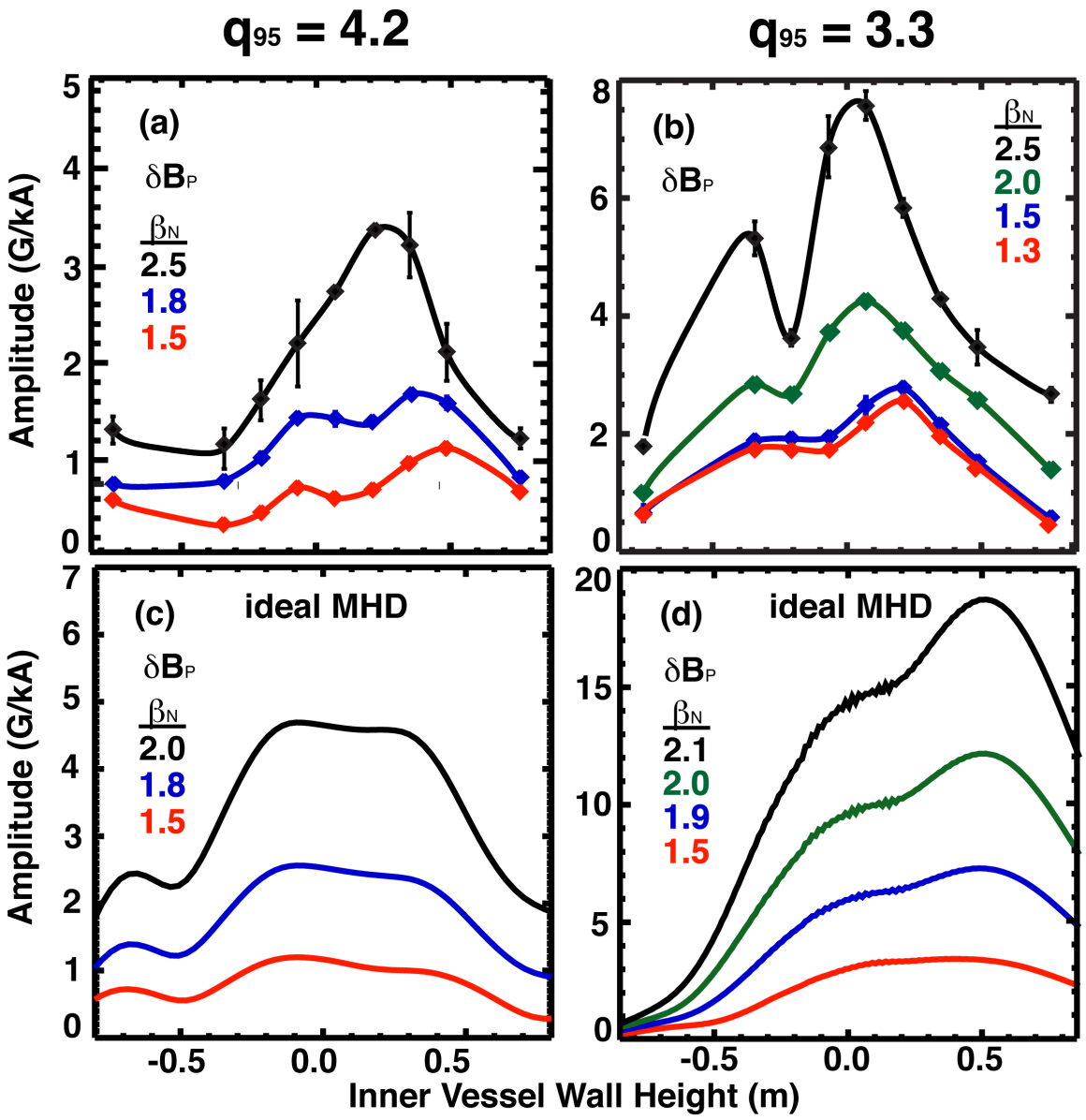
q95 = 4.2
q95 = 3.3
(a)
δBP
βN
2.5
1.8
1.5
(b)
δBP
βN
2.5
2.0
1.5
1.3
(c)
ideal MHD
δBP
βN
2.0
1.8
1.5
(d)
ideal MHD
δBP
βN
2.1
2.0
1.9
1.5
Amplitude (G/kA)
Amplitude (G/kA)
Inner Vessel Wall Height (m)

J.D. King Fig. 6

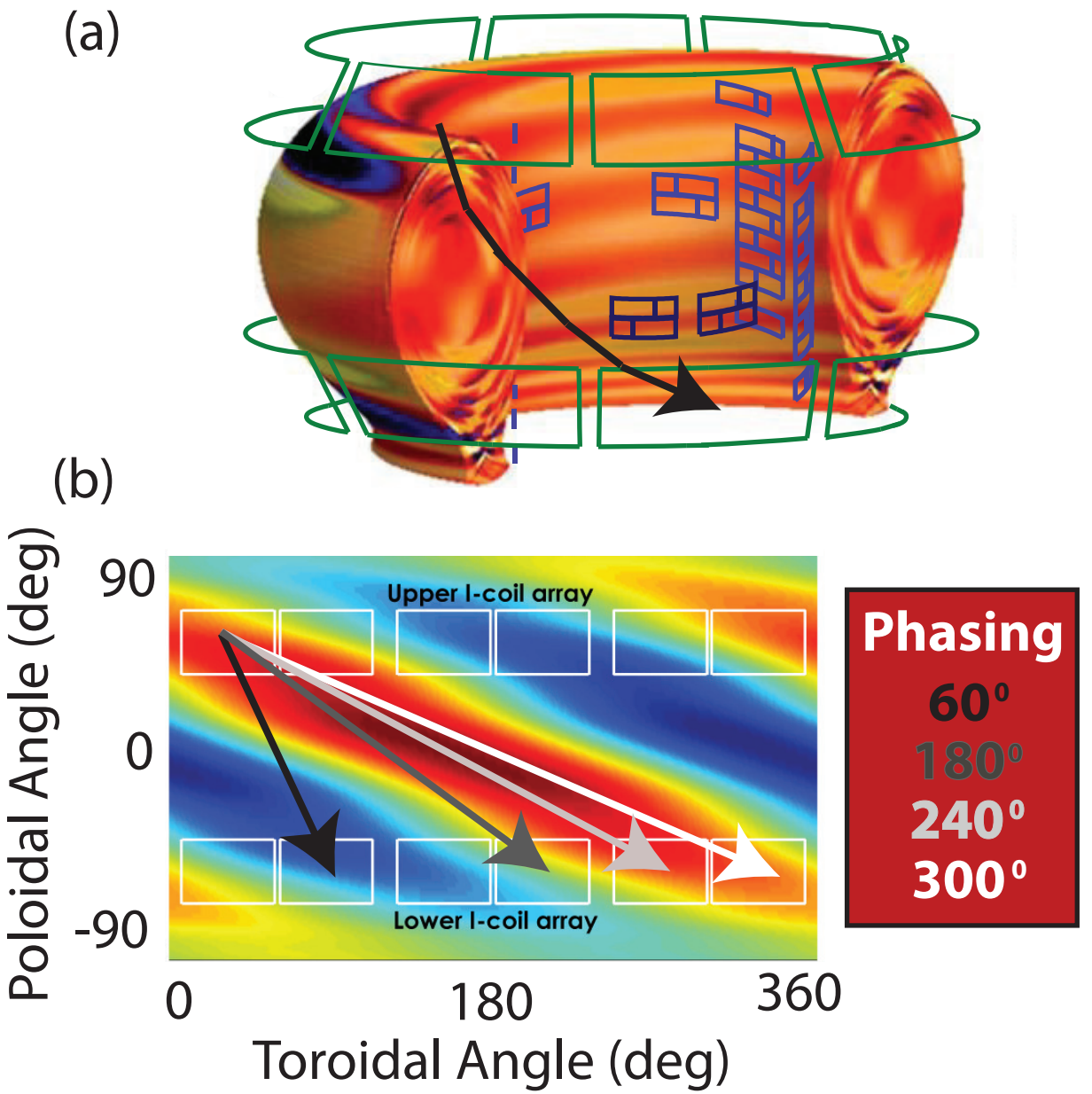
(a)
(b)
Poloidal Angle (deg)
90
0
-90
Upper I-coil array
Lower I-coil array
0
180
360
Toroidal Angle (deg)
Phasing
60°
180°
240°
300°

J.D. King Fig. 1

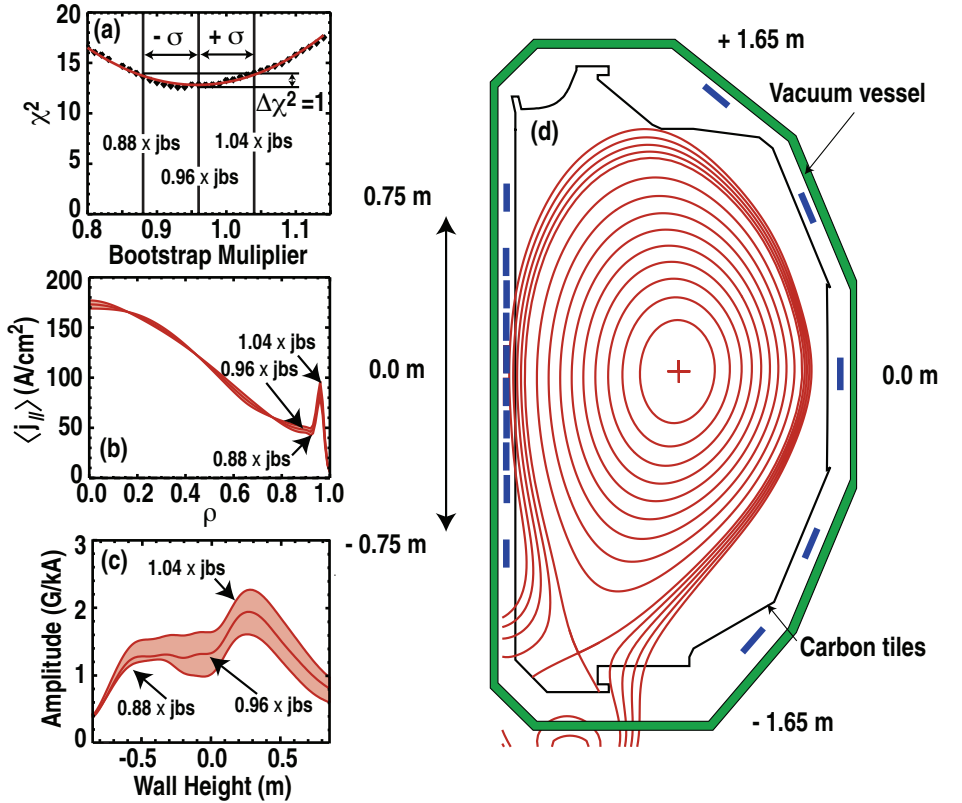
(a)
- σ
+ σ
χ^2
$\Delta\chi^2 = 1$
0.88 x jbs
1.04 x jbs
0.96 x jbs
Bootstrap Muliplier
(b)
$\langle j_{//} \rangle$ (A/cm^2)
1.04 x jbs
0.96 x jbs
0.88 x jbs
ρ
(c)
Amplitude (G/kA)
1.04 x jbs
0.88 x jbs
0.96 x jbs
Wall Height (m)
0.75 m
0.0 m
- 0.75 m
(d)
+ 1.65 m
Vacuum vessel
0.0 m
Carbon tiles
- 1.65 m

J.D. King Fig. 2

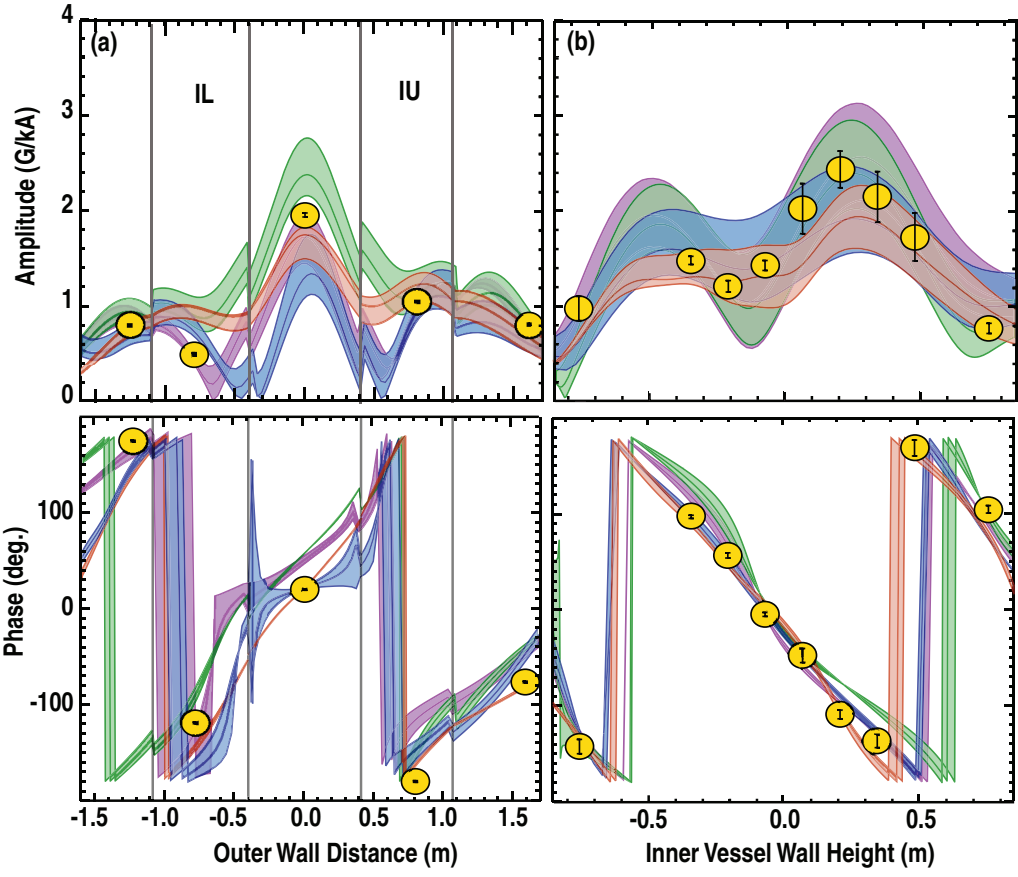
(a)
(b)
IL
IU
Amplitude (G/kA)
Phase (deg.)
Outer Wall Distance (m)
Inner Vessel Wall Height (m)

J.D. King Fig. 3

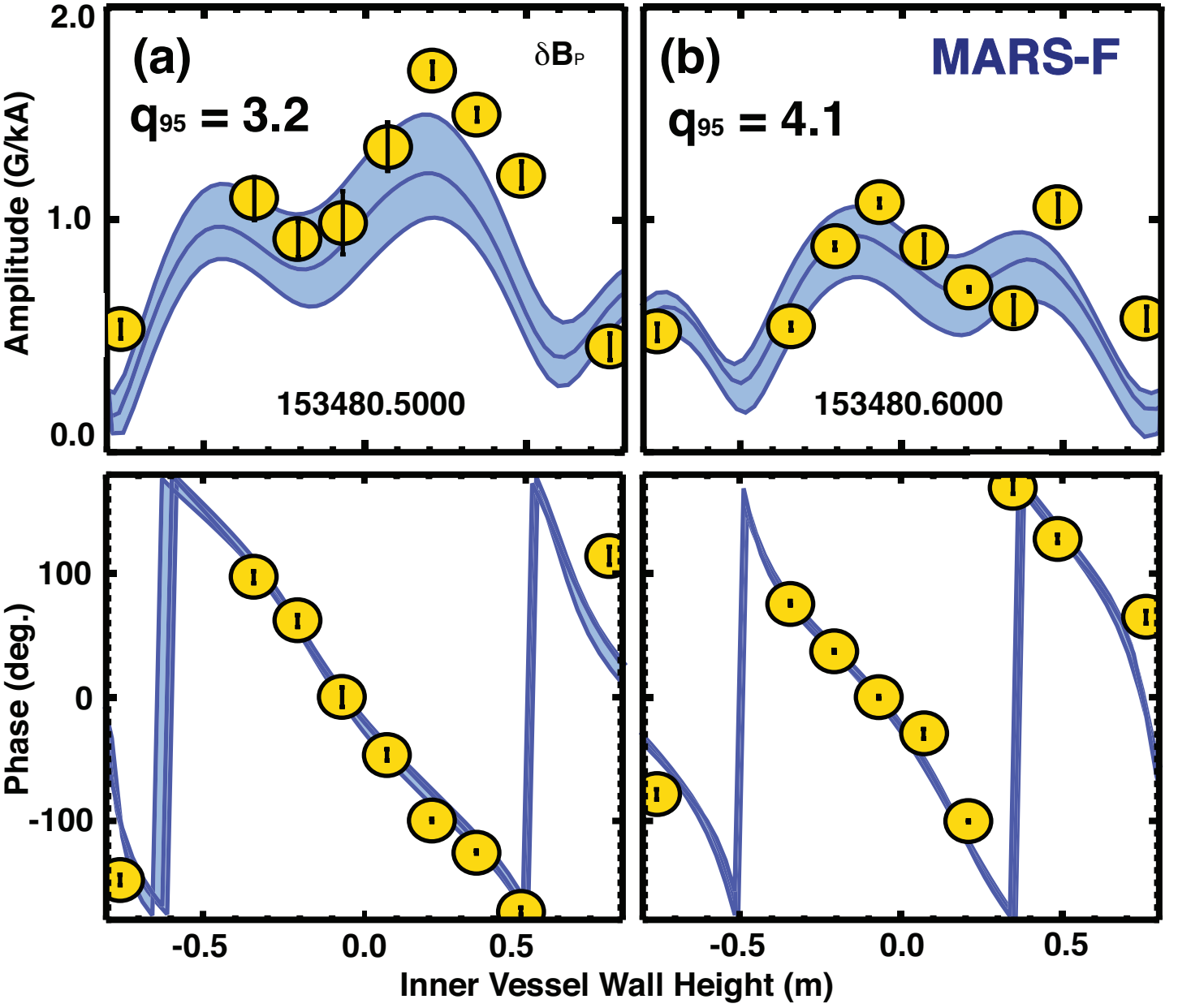
(a)
q_{95} = 3.2
δB_P
153480.5000
(b)
MARS-F
q_{95} = 4.1
153480.6000
Amplitude (G/kA)
2.0
1.0
0.0
Phase (deg.)
100
0
-100
-0.5
0.0
0.5
Inner Vessel Wall Height (m)

J.D. King Fig. 4

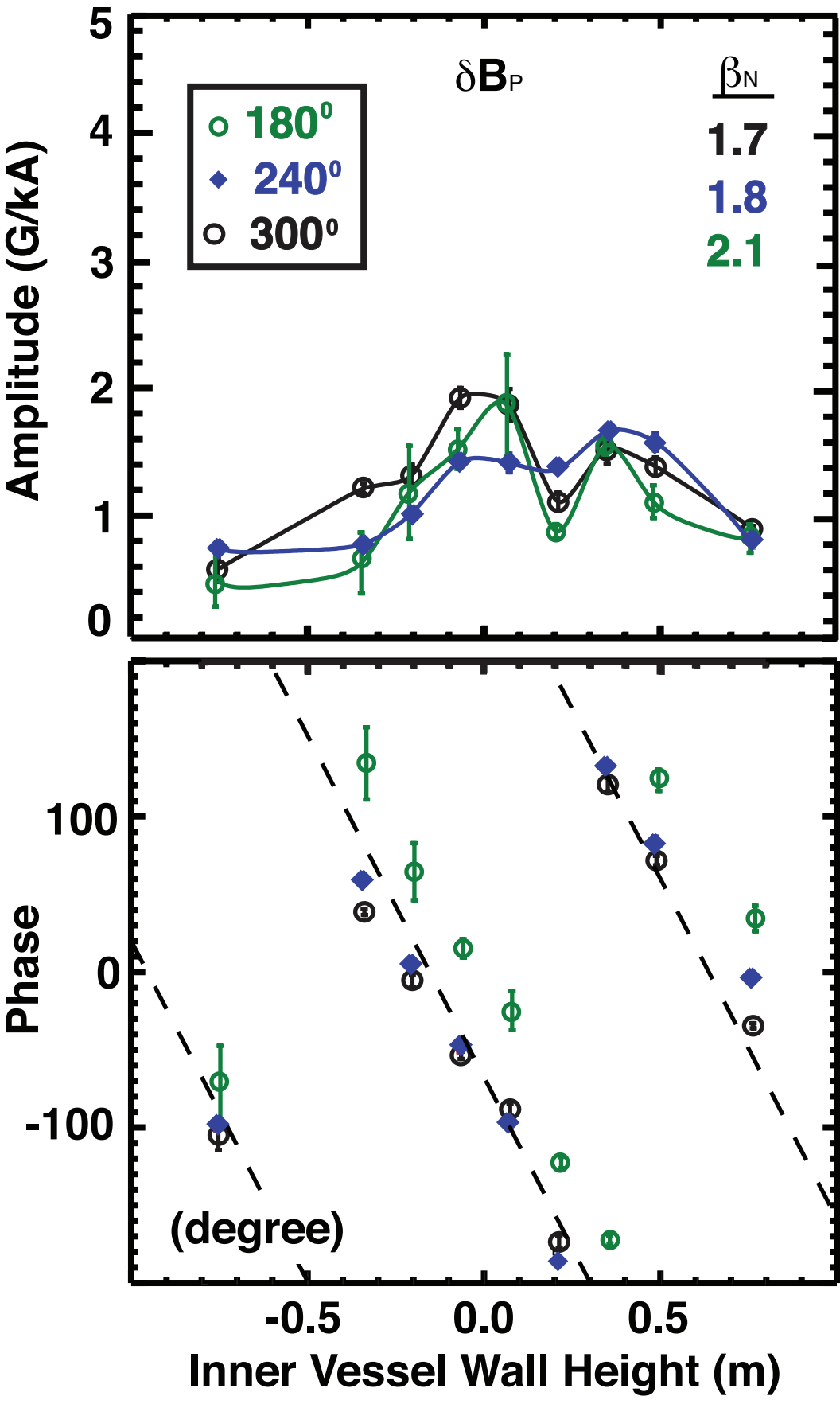
δBP
βN
1.7
1.8
2.1
180⁰
240⁰
300⁰
Amplitude (G/kA)
Phase
(degree)
Inner Vessel Wall Height (m)
5
4
3
2
1
0
100
0
-100
-0.5
0.0
0.5

J.D. King Fig. 5

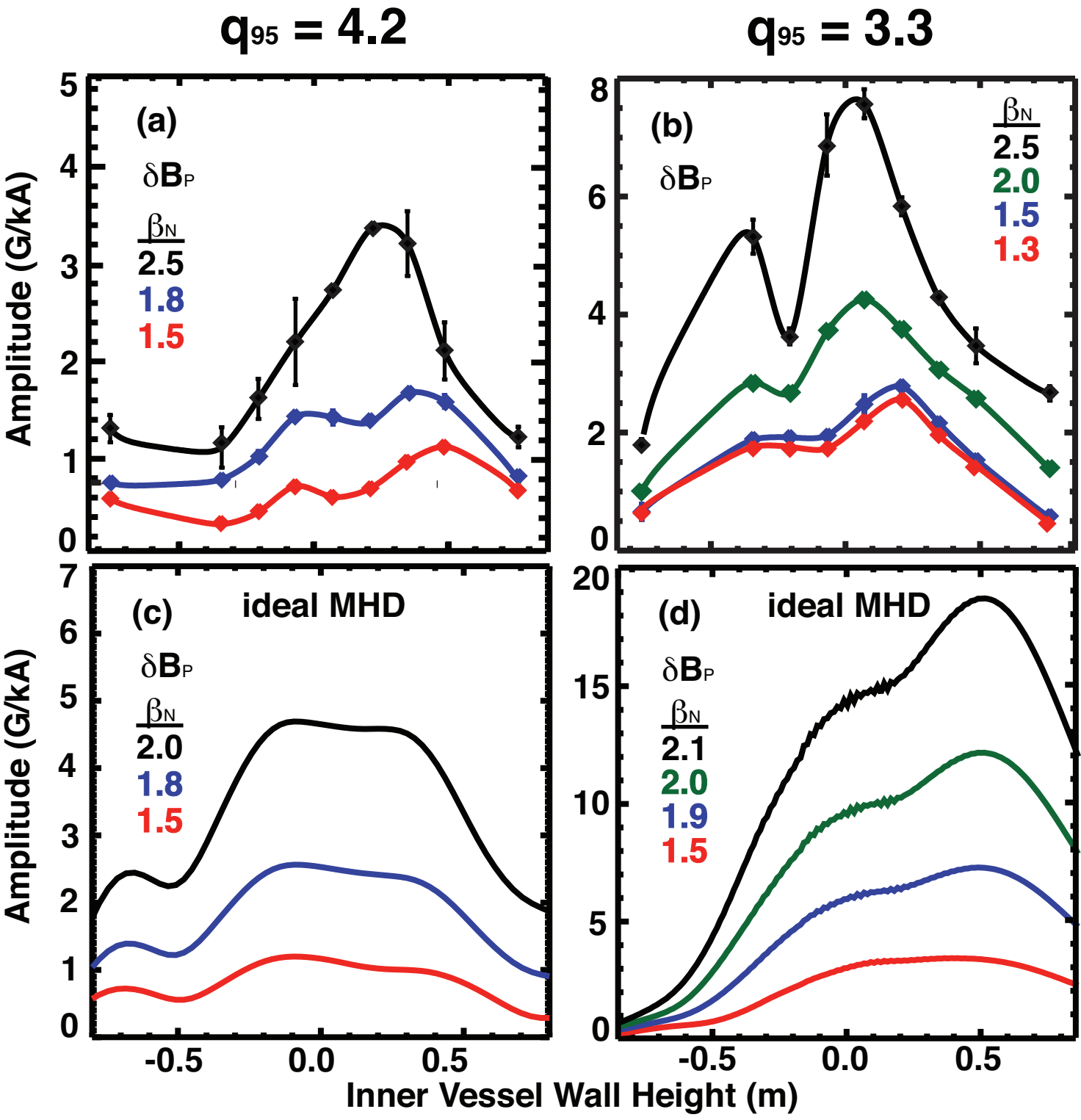
q95 = 4.2
q95 = 3.3
(a)
δBP
βN
2.5
1.8
1.5
(b)
δBP
βN
2.5
2.0
1.5
1.3
(c)
ideal MHD
δBP
βN
2.0
1.8
1.5
(d)
ideal MHD
δBP
βN
2.1
2.0
1.9
1.5
Amplitude (G/kA)
Amplitude (G/kA)
Inner Vessel Wall Height (m)

J.D. King Fig. 6